Macromolecules
ARTICLE

Macromolecules **2010**, *43*, 4331–4339 **4331**
DOI: 10.1021/ma100184h

Polyampholyte Microgels with Anionic Core and Cationic Shell

Susann Schachschal,[†] Andreea Balaceanu,[‡] Claudiu Melian,[‡] Dan E. Demco,[‡] Thomas Eckert,[§] Walter Richtering,[§] and Andrij Pich*,[‡]

[†]*Department of Macromolecular Chemistry, Technische Universität Dresden, D-01062 Dresden, Germany,* [‡]*DWI RWTH Aachen e.V., Institut of Technical and Macromolekular Chemistry, RWTH Aachen University, Pauwelsstr. 8, D-52056 Aachen, Germany, and* [§]*Institute of Physical Chemistry, RWTH Aachen University, Landoltweg 2, D-52056 Aachen, Germany*

Received January 25, 2010; Revised Manuscript Received April 6, 2010

ABSTRACT: We report synthesis of amphoteric microgels by copolymerization of *N*-vinylcaprolactam (VCL), itaconic acid dimethyl ester (IADME), and vinylimidazole (VIm) in the precipitation−polymerization process. After hydrolysis of ester groups of IADME, component microgels contain acidic and basic groups in their structure. Proton high-resolution transverse magnetization relaxation under magic angle sample spinning (MAS) was used to measure the dynamic heterogeneity corroborated with the chemical structure of a multicomponent amphoteric microgel. NMR results indicate that itaconic acid groups (originated from hydrolyzed IADME component) are localized mostly in the microgel core. The core−shell morphology of poly(*N*-vinylcaprolactam)-based microgels was suggested with carboxylic acid groups in the core and imidazole groups in the shell. The variation of the IADME and VIm content in microgel structure allows varying microgel charge and swelling degree in basic and acidic pH, respectively. Obtained amphoteric microgels exhibit narrow size distribution and superior colloidal stability.

1. Introduction

Aqueous colloidal microgels found useful applications in different areas such as coatings, agriculture, medicine, etc. Aqueous microgel particles with small dimensions present a unique class of nano-objects. Because of the cross-linked state, the interior is discriminated from the surface groups in accessability but also in chemical reactivity. The latter was caused by variations of local concentrations and polarity in the surrounding of the chemical groups inside the network and at the surface of the gel particles. Because of the hydrophilic nature of the constituent segments, nanoparticulate hydrogels are colloidally stable in water without need of adding surfactant molecules or polar surface modification. Because of their water solubility and water uptake, the microgel particles can take part in and experience short- and long-range interaction forces specific for aqueous systems, i.e., hydrophobic and electrostatic interactions.[1]

Aqueous microgels with defined size and size distribution can be prepared in form of stable colloids based on different polymers such as poly(*N*-isopropylacrylamide) (PNIPAAm),[2−6] poly(*N*-vinylcaprolactam) (PVCL),[7,8] poly(acrylic acid) (PAA),[9,10] poly(methacrylic acid) (PMA),[11] or poly(2-(diethylamino)ethyl methacrylate) (PDEA).[12] The special feature of PNIPAAm- or PVCL-based microgels is their sensitivity to temperature or pH changes that enables fabrication of "switchable" or "stimuli-responsive" materials.[13−20] Because of the small size and the large surface to volume ratio, the swelling/deswelling response to a change in temperature,[13,15] pH,[16,18−20] or ionic strength is fast and nearly instantaneously compared to macrogels.

The targeted design of the microgels, especially the incorporation of different functional groups and control over their distribution in microgel network, becomes more and more important in our days. In this context, the development of new techniques for the synthesis of amphoteric microgels is a challenging task, since it will allow obtaining multisensitive polymer colloids with unusual properties. So far, there exist several reports about synthesis of amphoteric microgels. The preparation methods can be divided into two groups: (a) polymerization processes and (b) self-assembly/cross-linking techniques.

The first group of preparation methods considers preparation of the microgels by free-radical copolymerization of different functional monomers[21−29] or by polyaddition reaction.[30] The free-radical polymerization processes have been realized in emulsion,[21,22] inverse miniemulsion,[23] or by precipitation−polymerization.[24−31] pH-responsive amphoteric core−shell microgel particles were synthesized by two-step emulsion polymerization of 2-(diethylamino)ethyl methacrylate and *tert*-butyl methacrylate.[22] The acid hydrolysis of ester groups in *tert*-butyl methacrylate was carried out to generate the methacrylic acid moieties in microgels. Amphoteric microgels were prepared by precipitation copolymerization of NIPAAm with acrylic acid and vinylimidazole.[24−26,28] Alternatively, Tan and co-workers prepared amphoteric colloids by copolymerization of acrylic acid, 2-(diethylamino)ethyl methacrylate, and poly(ethylene glycol) methyl ether methacrylate in aqueous phase.[29] Kawaguchi and co-workers used acrylamide, methacrylic acid, and 2-(diethylamino)ethyl methacrylate to prepare amphoteric microgels by semicontinuous precipitation−polymerization in ethanol.[30] The interfacial polyaddition reaction was carried out in the inverse miniemulsion system.[32] The reaction between L-lysine (localized in water droplets) with ethylene glycol diglycidyl ether dissolved in continuous medium (cyclohexane) led to the formation of amphoteric colloids bearing secondary amino and carboxyl groups.

The second group of methods for the preparation of amphoteric microgels utilizes self-assembly of different polymers followed by physical cross-linking. The cluster formation through self-assembly of β-casein and lysozyme was achieved in aqueous phase and polymer chains were physically cross-linked by heating-induced gelation.[33] In a similar manner amphoteric microgels based on ovalbumun and ovotransferrin were obtained.[34]

*To whom correspondence should be addressed.

Published on Web 04/15/2010

Kumacheva and co-workers used amphoteric microgels for sequestering of gold nanorods.[35] Amphoteric microgels have been also used as DNA scavengers. Taira and co-workers trapped ssDNA at neutral pH in amphoteric microgels due to the formation of the ion complex between negatively charged protein and positively charged colloids.[32] In alkaline pH ssDNa was released due to the electrostatic repulsion forces caused by the change of the microgel charge.

The amphoteric microgel systems reported in the literature exhibit randomly distributed ionizable groups within the polymer network. In this work we made an attempt to design amphoteric microgels with temperature-sensitive properties and controlled distribution of charged groups. To synthesize amphoteric microgels by precipitation−copolymerization process, we selected *N*-vinylcaprolactam as main monomer that provides temperature sensitivity as well as vinylimidazole (VIm) and dimethyl itaconate (IADME) (precursor for itaconic acid (IA)) as comonomers to ensure generation of positive or negative charges in microgel network. We selected itaconic acid because of its unique chemical properties, which derive primarily from the conjugation of one of its two carboxylic acid groups and its methylene group. The localization of two carboxylic acid groups in one monomer unit provides a very high theoretical ion-exchange capacity. As a result, microgels modified with IA may be effectively used for ion-exchange separation processes to extract cations such as metal ions, organic dyes, or proteins from solution.[36,37]

We have characterized this system using several methods (light scattering, electrophoretic mobility, electron microscopy, sedimentation velocity, NMR); however, the novelty in methodology comes from NMR, more exactly for using the differences in the transverse relaxation of functional groups to determine the morphology of the microgel particle. The results show a core−shell microstructure of the particles, with IA component mainly localized in the core. The separation of charges inside microgel particle offers a unique possibility to influence uptake/release processes based on electrostatic interactions, control chemical reactions within microgels, and design new nanostructured colloids.[38,39]

2. Experimental Part

2.1. Materials. *N*-Vinylcaprolactam (VCL), vinylimidazole (VIm) (Aldrich), and itaconic acid dimethyl ester or dimethyl itaconate (IADME) (Fluka) were purified by distillation under vacuum. Initiator 2,2′-azobis(2-methylpropionamidine) dihydrochloride (AMPA), cross-linker *N*,*N*′-methylenebis(acrylamide) (BIS) (Aldrich), and D_2O (99.9%, KMF GmbH, Germany) were used as received.

2.2. Synthesis of Microgels. Microgels were synthesized by placing appropriate amounts of VCL, IADME, VIm, and BIS (see Tables 1 and 2) into a 200 mL double-wall glass reactor equipped with a mechanical stirrer. The ingredients dissolved after addition of deionized water under stirring at 70 °C for 1 h under a nitrogen flow. Then the aqueous initiator solution was added dropwise into the reaction vessel, and the polymerization was carried out for 8 h. Polymerization was carried out at pH = 5. Stable microgel dispersions were obtained and were purified by dialysis (VIVA-Flow50, 50 000 MWCO, poly(ether sulfone)).

2.3. Hydrolysis Procedure. 0.1 M NaOH was slowly added to the microgel dispersion, and the mixture was stirred for 24 h. Then NaOH was neutralized with an equivalent amount of HCl, and the microgel sample was dialyzed for 4 days. The itaconic acid content was determined by potentiometrical titration.

2.4. Analytical Techniques. Microgel size and electrophoretic mobility were measured at 20 °C by using a Zeta-Sizer Nano ZS (Malvern Instruments). There are models to determine the zeta-potential for soft particles;[40] however, as the microgel prepared in this study has a rather complex internal structure, we decided to use the electrophoretic mobility instead of the often used zeta-potential. The pH was adjusted with an automatic titration unit using (0.25 M) NaOH and (0.25 M) HCl solutions.

Table 1. Ingredients Used for the Synthesis of VCL/IADME (VI) Microgels

sample	VCL [g]	IADME [g]	IADME [mol %]	BIS [g]	AMPA [g]	H_2O [g]
VI(1)	2.0589	0.0296	1.25	0.06	0.05	150
VI(2)	2.0329	0.0593	2.5	0.06	0.05	150
VI(3)	1.9808	0.1183	5.0	0.06	0.05	150
VI(4)	1.9286	0.1778	7.5	0.06	0.05	150
VI(5)	1.8765	0.2370	10.0	0.06	0.05	150
VI(6)	1.7723	0.3555	15.0	0.06	0.05	150
VI(7)	1.6704	0.4745	20.0	0.06	0.05	150

Proton NMR spectra of the VCL and IADME monomers as well as of the amphoteric microgels were measured on liquid-state Bruker NMR spectrometer operating at 600 MHz (see Supporting Information). The amphoteric gel ^{1}H NMR spectra were also measured on wide-bore Bruker NMR spectrometer operating at 700 MHz with a cross-polarization (CP) magic-angle sample spinning (MAS) probe head. The rotor frequency and the sample temperature were ν_R = 5 kHz and 22 °C, respectively. For all measurements the recycle delay was 5 s, the radio-frequency pulse length was 3.2 μs, and the dwell time of 10 μs was used. In the resulting NMR spectra we have identified resonances with the following chemical shifts: R_1 = 0.89 ppm; R_2 = 1.29 ppm; R_3 = 1.73 ppm; R_4 = 2.48 ppm; R_5 = 3.33 pmm; R_6 = 3.75 ppm. The assignment of these resonances to the microgel components and functional groups are discussed below (see also Supporting Information). The amphoteric microgel at pH = 5.6 was lyophilized by freeze-drying and redispersed in D_2O. Particle concentration was adjusted to 2 wt %.

The high-resolution MAS transverse relaxation (T_2) NMR measurements were made at 700 MHz proton frequency of a Bruker AV700 NMR spectrometer. For these measurements 2 wt % of the amphoteric microgel dissolved in deuterated water was used. The same rotor frequency, recycle delay, dwell time, and temperature as for ^{1}H spectra were employed. The decay of transverse magnetization relaxation was measured using Hahn-echo pulse sequence: $90°_x-t-180°_x-t-$Hahn echo (acquisition). Half of the Hahn echo decay was detected and Fourier transformed. The normalized integral intensities of various resonances were fit by single- and two-exponential decay functions using the Origin 6.0 program. The errors of the fits were smaller than 5%.

Electron microscopy (SEM) images were obtained with a Carl Zeiss instrument operating at 4 kV. Diluted microgel dispersions were placed onto glass substrates and dried at room temperature.

Sedimentation velocity of microgels samples was measured with an analytical centrifuge (LUM GmbH, Berlin) using a rotation speed of 3000 rpm. The slope of sedimentation curves (distance vs time) was used to calculate the sedimentation velocity and to get information about colloidal stability of the samples.

Dynamic light scattering (DLS) measurements were performed with a commercial laser light scattering spectrometer (ALV/DLS/SLS-5000) equipped with an ALV-5000/EPP multiple digital time correlator and laser goniometry system ALV/CGS-8F S/N 025 with a helium−neon laser (Uniphase 1145P, output power of 22 mW and wavelength of 632.8 nm) as a light source.

3. Results and Discussion

3.1. Microgel Synthesis. The synthesis of microgels was performed via batch precipitation polymerization route. The initial experiments were performed with VCL/IADME system (samples VI(1)−VI(7) Table 1) to find the optimal reaction conditions that allow obtaining colloidally stable

Table 2. Ingredients Used for the Synthesis of VCL/IADME/VIm (VIV) Microgels

sample	VCL:IADME [mol:mol]	VCL [g]	IADME [g]	VIm [g]	VIm [mol %]	BIS [g]	AMPA [g]	H_2O [g]
VIV(1)	85:15	1.7571	0.3523	0.0141	1	0.06	0.05	150
VIV(2)		1.7482	0.3505	0.0212	1.5	0.06	0.05	150
VIV(3)		1.7393	0.3487	0.0282	2	0.06	0.05	150
VIV(4)	90:10	1.8604	0.2349	0.0141	1	0.06	0.05	150
VIV(5)	80:20	1.6537	0.4697	0.0141	1	0.06	0.05	150

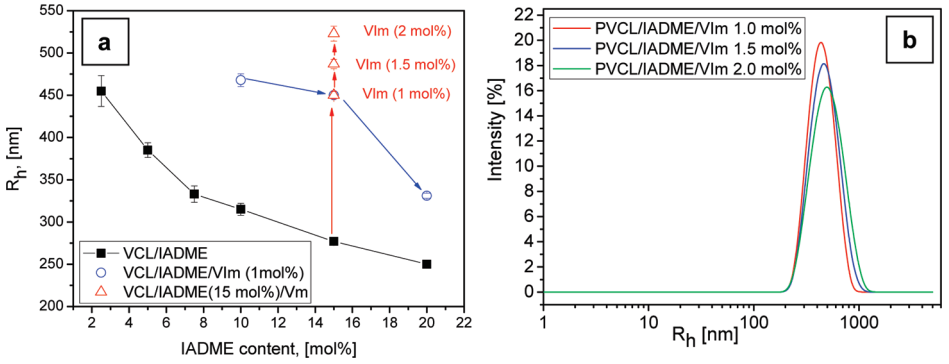

Figure 1. Hydrodynamic radii (R_h) as a function of IADME content in the microgel structure (a); particle size distribution curves for selected microgel samples (b) (T = 20 °C, pH = 5.6).

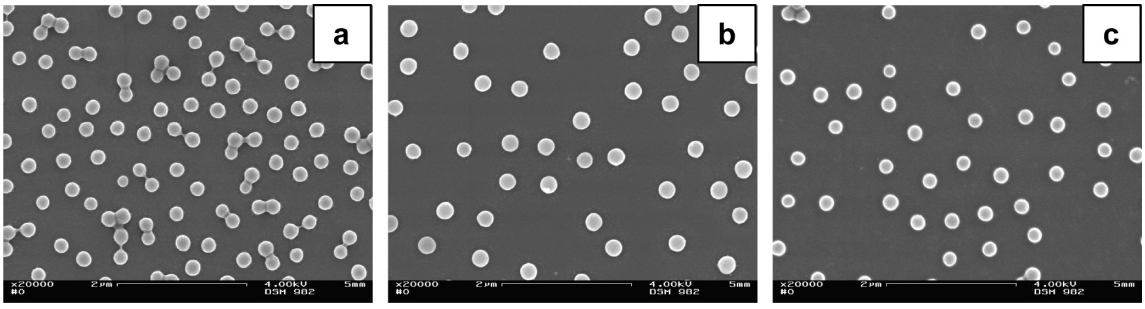

Figure 2. SEM images of VCL/IADME 15 mol %/VIm microgels: (a) 1 mol % VIm; (b) 1.5 mol % VIm; (c) 2 mol % VIm.

dispersion of monodisperse microgel particles. In this experiments the VCL:IADME monomer ratio was varied to obtain microgels with different amount of itaconate units. As shown in Figure 1, the hydrodynamic radii of microgel particles decrease with increase of the IADME content. Because of the higher reactivity and lower water solubility of IADME compared to VCL, we obtain microgels with the heterogeneous structure (IADME-rich core and VCL-rich shell). The reactivity ratios for vinylpyrrolidone VP(r_1) and IADME(r_2) were found $r_1 = 0.5$ and $r_2 = 1.3$, respectively.[41] In this study higher values of the reactivity ratios were obtained for dimethyl itaconate, indicating faster consumption during polymerization due to the preferable addition of this monomer to own and comonomer free radicals. In this situation formation of the copolymers with long sequences of dimethyl itaconate units was expected. A similar situation is expected in the VCL/IADME system since vinylcaprolactam and vinylpyrrolidone behave quite similarly, and this leads to the preferred localization of the IADME units in more compact microgel core surrounded by highly swollen VCL corona. The heterogeneous structure of the microgels was previously detected in microgels prepared by copolymerization of the more reactive acrylates (glycidyl methycrylate[42] or acetoacetoxyethyl methycrylate[43]) with VCL. The decrease of the microgel size with increase of the IADME content is due to the formation of more compact structure induced by lower solubility of itaconate units in water.

Further, we fixed the VCL:IADME monomer ratio and introduced vinylimidazole (VIm) into polymerization receipe (samples VIV1−VIV3). Vinylimidazole has similar copolymerization characteristics as VCL and high solubility in water, so those monomer units will be preferably integrated into the microgel corona. As shown in Figure 1a, the incorporation of VIm units in microgel structure induces rapid increase of the microgel size. The incorporation of the VIm leads to some broadening of the particle size distribution of the microgel particles shown in Figure 1b. In the last experiment series we prepared microgel samples with constant VIm content but different VCL:IADME ratio (samples VIV4 and VIV5). As shown in Figure 1a, the microgel size decreases with increase of the IADME content. In this way we obtained microgels with variable amount of IADME and VIm groups.

The SEM images for the VCL/IADME/VIm microgels with different copolymer composition in Figure 2 indicate that obtained microgels independently from the chemical composition possess narrow particle size distribution and spherical shape. SEM images of other microgel samples can be found in Supporting Information Figures S1 and S2.

After microgel synthesis ester groups of IADME were hydrolyzed to carboxylic groups (Figure 3). The hydrolysis degree was 80% for all microgel samples as determined by potentiometric titration. In this way we obtained microgels having carboxylic acid groups and imidazole groups incorporated into microgel network. Microgel samples were examined with SEM after hydrolysis procedure (Figures S3 and S4 in Supporting Information). No microgel destruction or broadening of the particle size distribution was detected

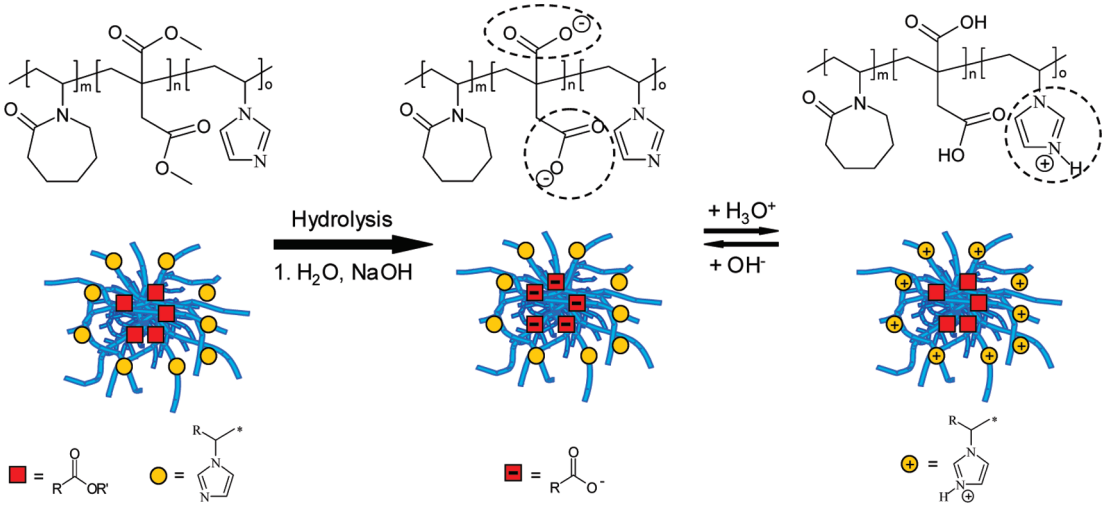

Figure 3. Schematic representation of polyampholyte microgels.

by electron microscopy and light scattering. After hydrolysis procedure and purification procedure (dialysis) microgels shrink considerably due to the partial charge neutralization at pH = 5.7 (Table S1 in Supporting Information).

3.2. Structure and Dynamic Heterogeneity of Microgels by ^{1}H Transverse Magnetization Relaxation. To confirm the heterogeneous microgel structure and investigate the distribution of acidic and basic functions in the microgel particles, we performed an NMR study. Proton NMR relaxometry, diffusometry, and measurements of the residual dipolar couplings were used in the past for characterization of the polymer networks structure and dynamics heterogeneities.[44−46] The structural inhomogeneities inside microgel particles of PNIPMAM were studied by ^{1}H transverse magnetization relaxation[47] without any ^{1}H resolution. The chain mobility for three different types of PNIPMAM gels (normal cross-linked, comb-type grafted gel, and comb-type grafted gel with styrene-modified comb chains) has been also investigated by ^{1}H transverse magnetization relaxation (T_2).[48]

The heterogeneity in the microgel morphology would be reflected in the ^{1}H transverse magnetization relaxation due to different degree of local molecular motions correlated to the distribution in cross-link density. From T_2 decays we can show that a bimodal distribution of molecular dynamics is essentially present from which the morphological model of core−shell could be derived.

In our study we applied ^{1}H high-resolution transverse magnetization relaxation made under MAS with a high-field NMR spectrometer at 16.44 T that allows study of the dynamics and structure heterogeneity of amphoteric microgels. To study the distribution of monomer units in microgel by NMR, the hydrolyzed microgel sample VIV(1) (Table 1) was used. A proton high-resolution NMR MAS spectrum of this sample was recorded (Figure 4), and the resonance assignments were made using the ^{1}H simulated spectra obtained with the Gaussian03 Simulation Package and ^{1}H liquid-state spectra of monomers measured with a 600 MHz Bruker NMR spectrometer (see Supporting Information Figure S5). The R_2, R_3, R_4, and R_6 resonances in Figure 4 can be assigned to VCL and R_5 to itaconic acid (IA) components. The MAS spectra show improved spectral resolution as compared to the ones measured under the static conditions.

The proton Hahn-echo decays measured chemically site selective are shown in Figure 5 for the resonance R_4 corresponding to VCL and R_5 assigned to IA.

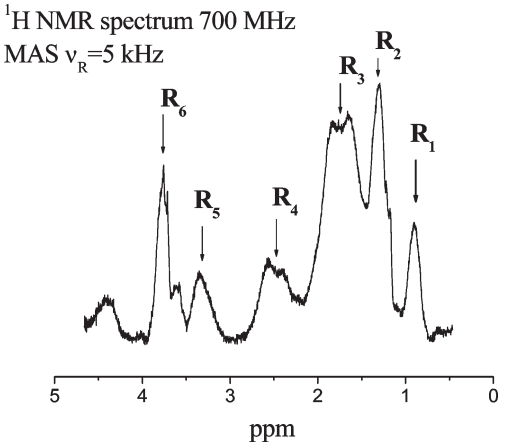

Figure 4. Proton high-resolution spectrum of amphoteric microgel (sample VIV(1): VCL:IA = 85:15; 1 mol % VIm) at 22 °C. The spectrum was measured at 700 MHz NMR spectrometer under MAS conditions (ν_R = 5 kHz).

We assume a biexponential decay for the R_4 resonance (Figure 5a), i.e.

$$\frac{S(t)}{S(0)} = c_1 \exp\left\{-\frac{t}{T_{2s}}\right\} + c_2 \exp\left\{-\frac{t}{T_{2l}}\right\} \qquad (1)$$

where $S(t)/S(0)$ is the normalized NMR signal integral as a function of spin−echo time t and c_i (i = s and l) are the relative contribution of the decays characterized by short (T_{2s}) and long (T_{2l}) transverse relaxation times. The fit with two exponentials (eq 1) has χ^2 = 0.001 12 and a coefficient of correlation of R^2 = 0.991 12. Hence, the fit is quantitative, and the relative weight of the two exponentials are c_1 = 26% and c_2 = 74%. These coefficients describe quantitatively the heterogeneity of the polymer network in the microgel. The fit with a sum of three exponentials leads to large errors in the fit parameters. Furthermore, the decay of the spin−echo NMR signal of resonance R_5 (Figure 5b) can be fitted only with a monoexponential decay, i.e.

$$\frac{S(t)}{S(0)} = c \exp\left\{-\frac{t}{T_2}\right\} \qquad (2)$$

The values of the ^{1}H transverse relaxation times for R_4 and R_5 resonances are shown in Figure 6. It is well-known from

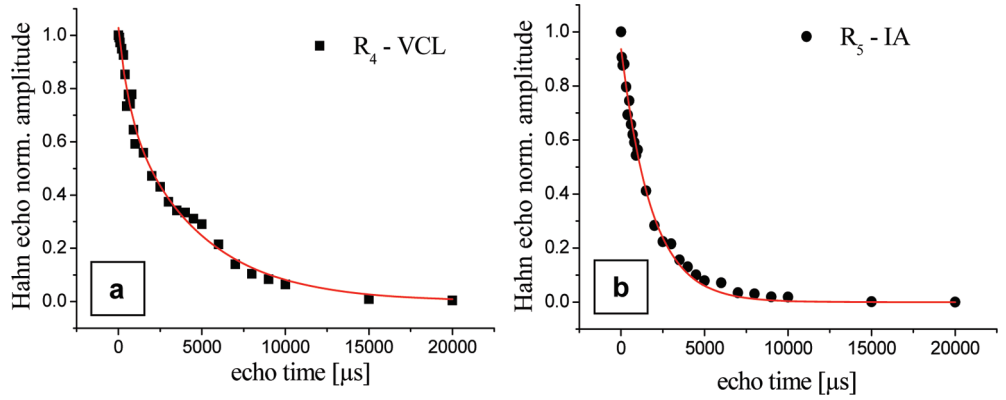

Figure 5. Hahn-echo decays of the integral intensities of the resonances R_4 (a) and R_5 (b) corresponding to VCL and IA, respectively. The best fits shown by solid lines were made with a sum of two exponentials (a) and a monoexponential (b). The measurements were made at 22 °C under MAS (ν_R = 5 kHz).

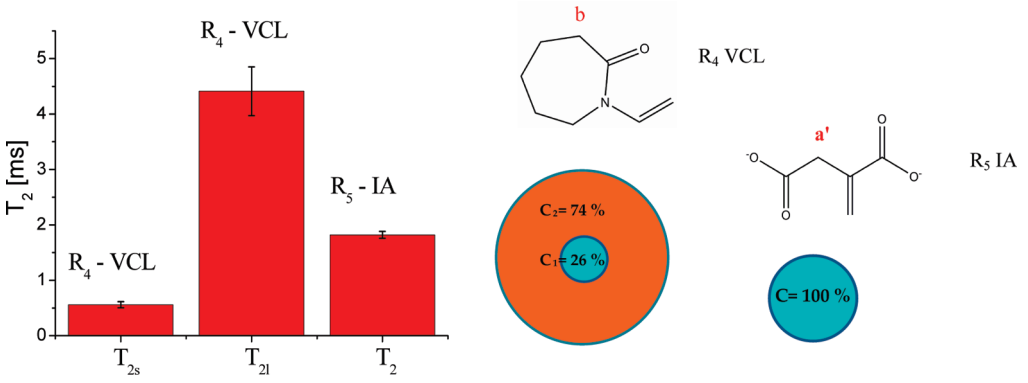

Figure 6. (a) Transverse relaxation times (T_2) of amphoteric microgel. A short (T_{2s}) and a long (T_{2l}) transverse relaxation times were obtained for the resonance R_4 (proton *b* of VCL). A single T_2 was measured for the R_5 resonance (proton *a*′ of IA). Drawings on the right-hand side show schematically distribution of VCL and IA in microgel. The dimensions of core and corona are not to scale.

the NMR relaxometry of polymer networks[44,49] that the transverse relaxation is strongly affected by the degree of the cross-link density via residual dipolar couplings and their fluctuations. The value of $T_{2s} \approx 0.5$ ms corresponds to a network with a larger value of the cross-link density as compared to $T_{2l} \approx 4.5$ ms. Local functional groups dynamics and the fluctuation of dipolar network contribute together to the T_2 values. The R_5 resonance decay of IA protons is characterized by a single T_2 with the value intermediate between those of R_4 protons of VCL (Figure 5). This could be explained *inter alia* by the weaker residual dipolar couplings of *a*′ proton of IA as compared to that of *b* proton of VCL (Figure 6, left-hand side). The local motions of the proton *a*′ have larger frequencies and amplitude due to rotational isomerization transitions and segmental motions compared to the proton *b* of VCL.

The biexponential decay of the R_4 resonance of VCL can be interpreted as probing the heterogeneity of the VCL distribution in the microgel. A core−shell morphology is detected with the relative proton content of VCL of c_1 = 26% and c_2 = 74% of the core and shell, respectively (Figure 6, right-hand side). The T_2 value of the IA protons being close to the T_{2s} shows that IA is mainly localized in the core.

Considering peculiarities of the polymerization process discussed previously (different reactivity and water solubility of the monomers) and NMR results, we conclude that obtained microgels possess a heterogeneous structure: compact IA-rich core and VCL corona decorated with VIm groups.

3.3. pH-Sensitive Properties. The sensitivity of the microgels to pH was studied by measuring the particle size at different pH values. The ionization of itaconic acid groups or imidazole groups in basic and acidic pH respectively should result in the increase of the microgel size due to the electrostatic repulsion forces and induced particle swelling. Figure 7 shows a summary of experimental data for microgel samples with nonhydrolyzed and hydrolyzed IADME units.

Nonhydrolyzed microgel samples swell in acidic pH and increase their size (maximum swelling detected at pH = 4.5). In the basic region microgel size remains constant because IADME units do not generate any charge (Figure 7a,c). The variation of the VIm content in the microgels led to the increase of the microgel swelling at pH = 4.5 (Figure 7a). In the case when IADME content was varied the swelling of the microgel samples at pH = 4.5 remains almost constant.

The microgel samples with IA units (hydrolyzed IADME) exhibiting carboxylic acid groups show amphoteric behavior; e.g., these particles swell in both acidic and basic regions (Figure 7b,d). The maximal swelling of amphoteric microgels was detected at pH = 8. The variation of the VIm and IA content in microgel networks allow tuning the pH-induced swelling of microgels. The reduction of the size of the microgels at extreme pH is attributed to the high ionic strength of the solution. This effect results in charge screening and reduction of repulsive electrostatic forces in the microgel particles.[22,28] All investigated microgel samples remain colloidally stable at different pH, and no particle aggregation was detected.

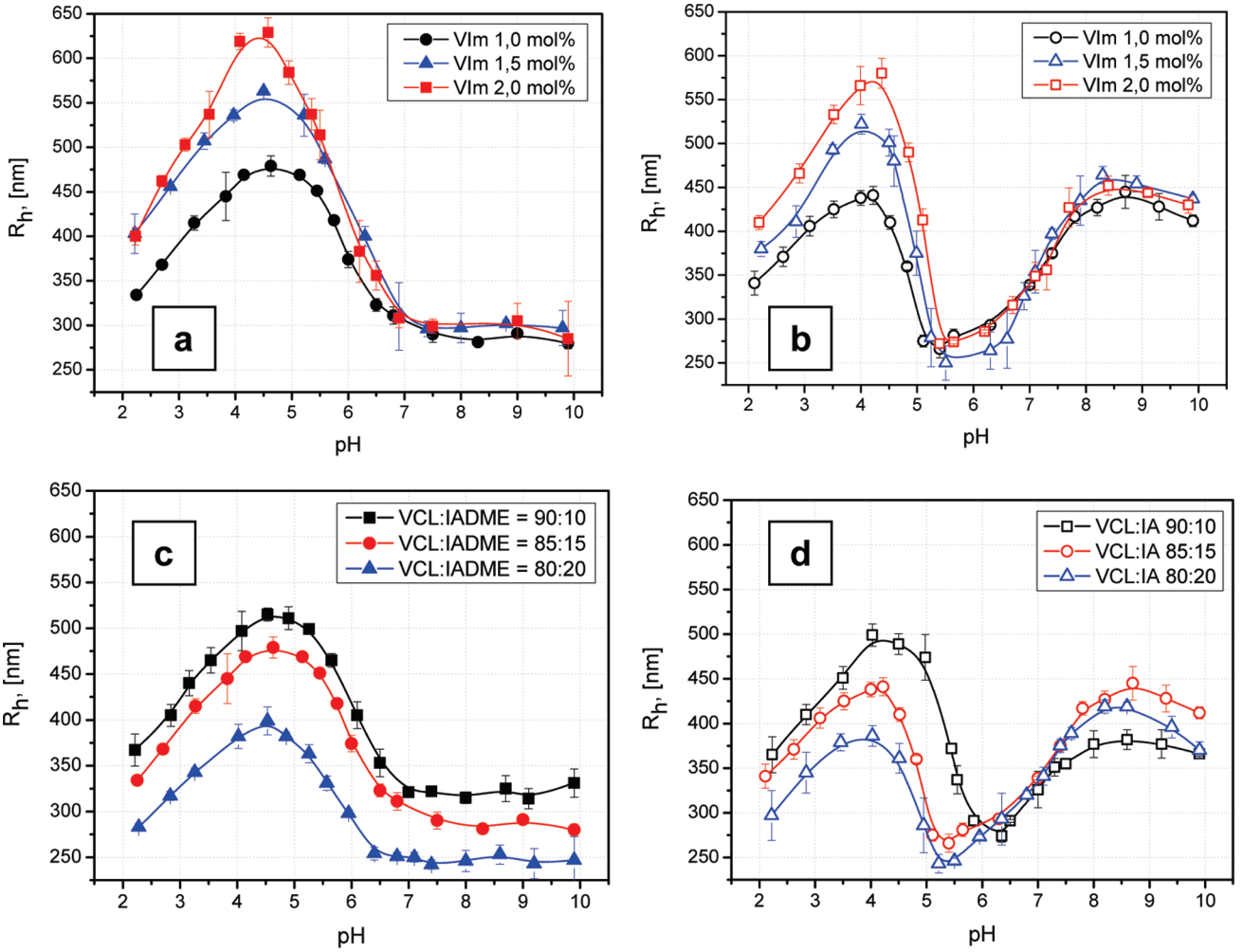

Figure 7. Hydrodynamic radii of nonhydrolyzed (a, c) and hydrolyzed (b, d) microgels as a function of pH.

In analogy to light scattering experiments described before, the electrophoretic mobility was measured for nonhydrolyzed and amphoteric (hydrolyzed) microgel samples as a function of pH. The experimental results in Figure 8 indicate that nonhydrolyzed samples exhibit positive surface charge in acidic pH range with a maximum of positive charge at pH = 4.5. This correlates with results of light scattering experiments (Figure 7a,c) that indicate the maximal microgel swelling and largest hydrodynamic radii at pH = 4.5. In pH range 7−10 microgels possess very weak negative charge which is not changing with pH. Contrarily, amphoteric microgels switch their charge from positive to negative by changing the pH from acidic to basic (Figure 8b,d). It is obvious from Figure 8b,d that the variation of the VIm or IA units in the microgel structure allows to tune microgel charge in acidic and basic region, respectively. Comparing parts b and d of Figure 8, we note that the position of isoelectric point for microgel samples with variable composition is different. For microgel samples with variable VIm content the isoelectric point is located at pH = 5.6. In the case of microgel with variable IA content the isoelectric point is shifted to higher or lower pH with increase or decrease of IA content, respectively. The isoelectric point of polyampholytes shifts as a function of copolymer composition.[50] The decrease of isoelectric point with increase of the poly(methacrylic acid) content in amphoteric poly(methacrylic acid)-(2-(dimethylamino)ethyl methacrylate) microgels was observed by Ho and co-workers.[51] Bradley et al.[52] reported shift of the isoelectric point to higher pH values with increase of the amine:carboxylic acid ratio in poly(2-(diethylamino)ethyl methacrylate-*co*-methacrylic acid) microgel particles. The shift of the isoelectric point toward lower values of pH with the increase of the acrylic acid (AA) content in amphoteric PNIPAAm/AA/VIm microgels was reported by Das et al.[28] This effect was explained by partial neutralization of COO^- groups by $=NH^+$ moieties what requires higher acidity to protonate the excess of COO^- groups to reach the isoelectric point.

Because of the presence of VCL obtained, amphoteric microgels exhibit temperature-sensitive properties. Microgels are in swollen state at room temperature and start to collapse upon heating (if temperature is increased above the volume phase transition temperature). In Figure 9a we present as an example light scattering data illustrating the temperature-sensitive behavior of microgel samples with variable VIm content. At pH = 4, due to the presence of charged VIm groups, the transition region is shifted toward higher temperatures compared to the T_{tr} = 35 °C observed in neutral PVCL-based microgel systems.[43] At high temperatures microgels are in collapsed state and possess hydrodynamic radius of 150 nm. The ratio $R_h^{60\,°C}/R_h^{20\,°C}$ can be used to describe the temperature-induced microgel shrinkage. As shown in Figure 9b, amphoteric microgels change their dimensions upon heating in acidic and basic pH. Interestingly, at pH = 5.6 microgels are in swollen state but nearly not sensitive to temperature. Measured hydrodynamic radii

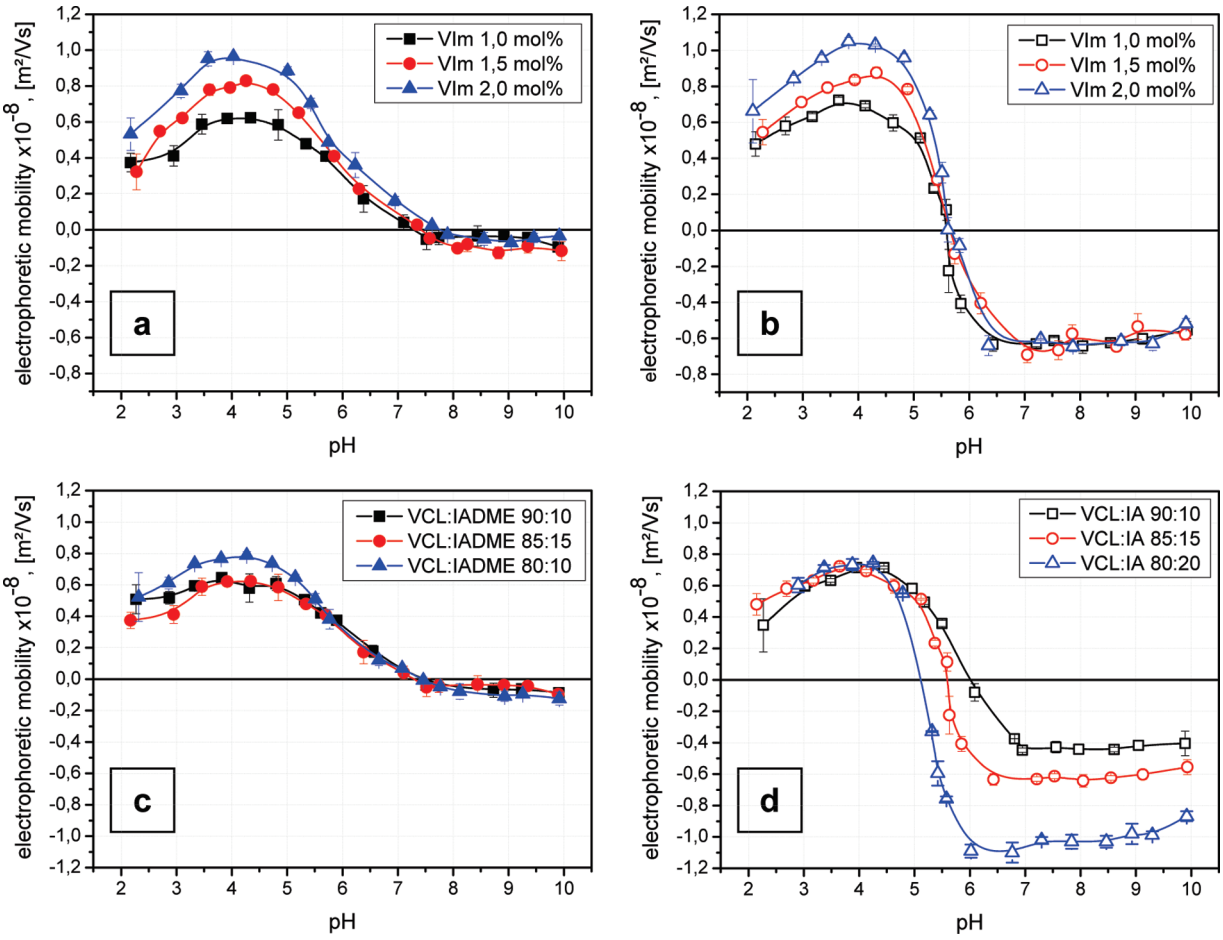

Figure 8. Electrophoretic mobility of microgels as a function of pH.

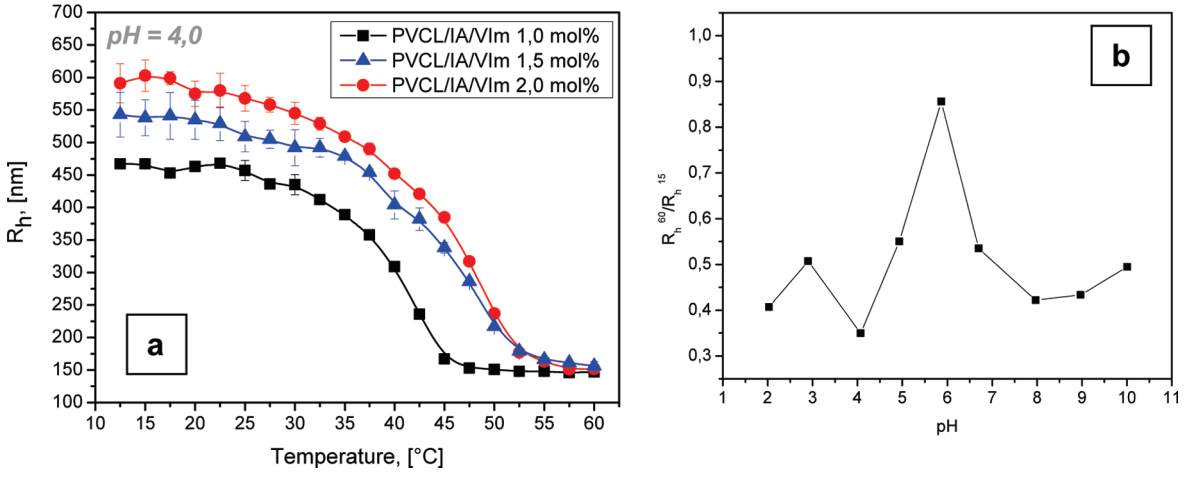

Figure 9. Hydrodynamic radii of microgel samples measured at different temperatures (a). Calculated $R_h^{60\,°C}/R_h^{20\,°C}$ ratio for sample VIV(1) (Table 1) as a function of pH (b).

are 250 and 210 nm at 20 and 60 °C, respectively. Therefore, the $R_h^{60\,°C}/R_h^{20\,°C}$ ratio reaches maximum at this pH. As is shown in Figure 8b at pH = 5.6 microgels exhibit isoelectric point, and the charge compensation between polymer segments probably leads to formation of ionic complexes. This reduces considerably the mobility of polymer chains and results in a "frozen" structure where electrostatic interactions overcome hydrophobic forces responsible for the microgel collapse at high temperatures. These microgels thus provide a very interesting comparison to ionic complexes of charged microgels and oppositely charged polyelectrolytes which also display peculiar properties as a function of pH and temperature.[53]

3.4. Colloidal Stability. To investigate colloidal stability of amphoteric microgels, we used a separation analyzer that allows detecting the sedimentation of microgels in centrifugal field. Figure 10a,b shows experimental curves showing the position of particle sedimentation front (defined as distance from the rotor center to the phase boundary between supernatant and sediment) at different sedimentation

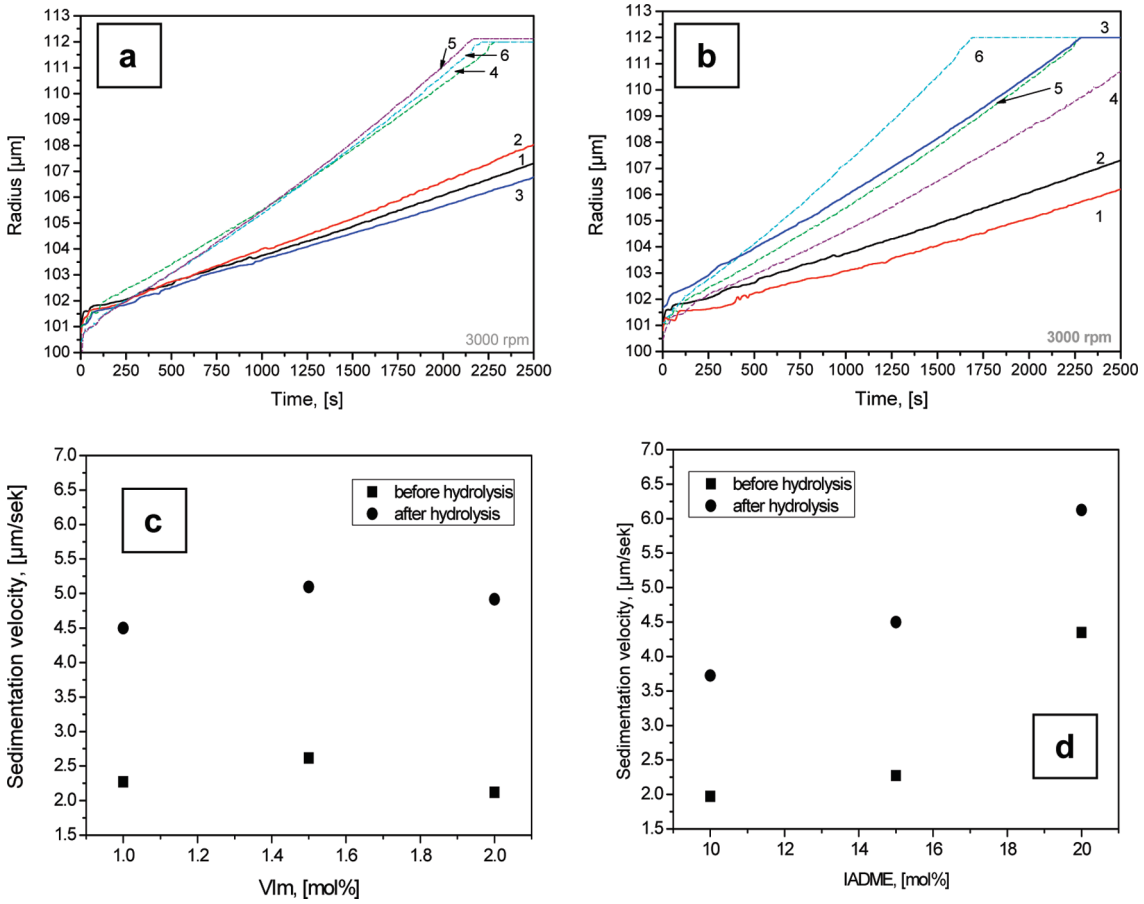

Figure 10. Sedimentation curves for microgel samples: (a) 1, VIV(1); 2, VIV(2); 3, VIV(3) (before hydrolysis) and 4, VIV(1); 5, VIV(2); 6, VIV(3) (after hydrolysis); (b) 1, VIV(4); 2, VIV(1); 3, VIV(5) (before hydrolysis) and 4, VIV(4); 5, VIV(1); 6, VIV(5) (after hydrolysis). Sedimentation velocity data (c) and (d) (calculated from (a) and (b), respectively) for nonhydrolyzed and hydrolyzed microgel samples with different compositions (T = 20 °C; pH = 5.7; rotation speed 3000 rpm).

times for nonhydrolyzed and hydrolyzed (amphoteric) microgel samples. The increase of the radius with time indicates that microgel particles precipitate under centrifugal force, and the plateau value is reached when the sedimentation process is completed. The slope of the radius vs time curves is used to calculate the sedimentation velocity (Figure 10c,d). The general conclusion from experimental data in Figure 10 is that hydrolyzed samples (amphoteric microgels) exhibit higher sedimentation velocities and lower colloidal stability compared with nonhydrolyzed samples. The experiment was performed at pH = 5.7, and in this case amphoteric microgels are close to their isoelectric point. Therefore, the electrostatic contribution to the microgel stabilization is reduced due to the charge compensation. Contrary, nonhydrolyzed samples exhibit weak positive charge from VIm units at pH = 5.7, and microgel stabilization occurs through electrosterical mechanism.

Comparing the results in Figure 10c,d, we note that the colloidal stability of microgels is nearly not influenced by the amount of VIm units. Contrarily, the increase of IA content in microgels results in higher sedimentation velocity values and lower colloidal stability. This can be explained by increase of the particle density due to the incorporation of IADME in the microgel core. We observed similar effect for the microgel system based on VCL and acatoacetoxyethyl methacrylate (AAEM).[43] In this case microgel particles with higher amount of AAEM localized in the core showed higher sedimentation velocities.

To investigate the influence of pH on the colloidal stability of microgels, we analyzed microgel samples with different IA content. The experimental results presented in Table 3 show that amphoteric microgels exhibit much lower sedimentation velocities at pH = 4 and pH = 8 compared to pH = 6. The protonization of VIm an IA groups in acidic and basic pH range led to enhanced stabilization of microgels in aqueous medium by electrosterical mechanism.

Table 3. Sedimentation Velocity Data as a Function of pH

	sedimentation velocity [μm/s]		
IA [mol %]	pH = 4	pH = 6	pH = 8
10	1.353	3.724	1.683
15	2.374	4.501	2.964
20	4.569	6.127	2.611

4. Conclusions

In this paper we report synthesis of monodisperse microgel system based on copolymer of *N*-vinylcaprolactam (VCL), itaconic acid dimethyl ester (IADME), and vinylimidazole (VIm). Microgels with different amounts of VIm and IADME have been synthesized by the precipitation−polymerization process. After hydrolysis of ester groups of IADME, we obtained amphoteric microgels having carboxylic (IA) and basic (VIm) groups in polymer network. Proton high-resolution transverse magnetization relaxation was shown for the first time to be able to investigate dynamics and structural heterogeneity in a multicomponent microgel. For the specific case of this amphoteric microgel core−shell morphology was detected with carboxylic groups located in the core and VIm groups located in PVCL corona. Obtained microgel particles exhibit polyampholyte behavior.

The electrostatic repulsion force induces microgel swelling in acidic and basic pH due to the protonization of imidazole and carboxylic acid groups, respectively. Amphoteric microgels exhibit superior colloidal stability at different pH.

Acknowledgment. The authors thank Deutsche Forschungsgemeinschaft (DFG) and VolkswagenStiftung for financial support of this research. A.B. acknowledges the financial support by the excellence initiative of the German federal and state governments.

Supporting Information Available: SEM images of microgels, ^{1}H NMR spectra of monomers, cryo-TEM images of microgels, potentiometrical titration, sedimentation analysis. This material is available free of charge via the Internet at http://pubs.acs.org.

References and Notes

(1) Pelton, R. *Adv. Colloid Interface Sci.* **2000**, *85*, 1.
(2) Park, T. G.; Hoffman, A. S. *Biotechnol. Prog.* **1994**, *10*, 82.
(3) Berndt, I.; Richtering, W. *Macromolecules* **2003**, *36*, 8780.
(4) Tauer, K.; Gau, D.; Schulze, S.; Volkel, A.; Dimova, R. *Colloid Polym. Sci.* **2009**, *287*, 299.
(5) Liu, R.; Fraylich, M.; Saunders, B. R. *Colloid Polym. Sci.* **2009**, *287*, 627.
(6) Nayak, S.; Lyon, L. A. *Angew. Chem., Int. Ed.* **2005**, *44*, 7686.
(7) Peng, S. F.; Wu, C. *Macromol. Symp.* **2000**, *159*, 179.
(8) Boyko, V.; Pich, A.; Lu, Y.; Richter, S.; Arndt, K.-F.; Adler, H.-J. *Polymer* **2003**, *44*, 7821.
(9) Bromberg, L.; Temchenko, M.; Hatton, T. A. *Langmuir* **2002**, *18*, 4944.
(10) Bromberg, L.; Temchenko, M.; Hatton, T. A. *Langmuir* **2003**, *19*, 8675.
(11) Eichenbaum, G. M.; Kisetr, P. F.; Shah, D.; Meuer, W. P.; Needham, D.; Simon, S. A. *Macromolecules* **2000**, *33*, 4087.
(12) Amalvy, J. I.; Wanless, E. J.; Li, Y.; Michailidou, V.; Armes, S. P.; Duccini, Y. *Langmuir* **2004**, *20*, 8992.
(13) Debord, J. D.; Lyon, L. A. *Langmuir* **2003**, *19*, 7662.
(14) Jones, C. D.; Lyon, L. A. *Langmuir* **2003**, *19*, 4544.
(15) Ogawa, K.; Nakayama, A.; Kokofuta, E. *J. Phys. Chem. B* **2003**, *107*, 8223.
(16) Pinkrah, V. T.; Snowden, M. J.; Mitchell, J. C.; Seidel, J.; Chowdhry, B. Z.; Fern, G. R. *Langmuir* **2003**, *19*, 585.
(17) Hoare, T.; Pelton, R. *Langmuir* **2004**, *20*, 2123.
(18) Hoare, T.; Pelton, R. *Macromolecules* **2004**, *37*, 2544.
(19) Peng, S.; Wu, C. *Macromolecules* **2001**, *34*, 6795.
(20) Peng, S.; Wu, C. *Polymer* **2001**, *42*, 6871.
(21) Hampton, K. W., Jr.; Ford, W. T. *Macromolecules* **2000**, *33*, 7292.
(22) Christodoulakis, K. E.; Vamvakaki, M. *Langmuir* **2010**, *26*, 639.
(23) Neyret, S.; Vincent, B. *Polymer* **1997**, *38*, 6129.
(24) Ito, S.; Ogawa, K.; Suzuki, H.; Wang, B.; Yoshida, R.; Kokofuta, E. *Langmuir* **1999**, *15*, 4289.
(25) Ogawa, K.; Nakayama, A.; Kokufuta, E. *Langmuir* **2003**, *19*, 3178.
(26) Ogawa, K.; Nakayama, A.; Kokufuta, E. *J. Phys. Chem. B* **2003**, *107*, 8223.
(27) Nayak, S. P.; Lyon, L. A. *Polym. Prepr.* **2003**, *44*, 679.
(28) Das, M.; Kumacheva, E. *Colloid Polym. Sci.* **2006**, *284*, 1073.
(29) Tan, B. H.; Ravi, P.; Tam, K. C. *Macromol. Rapid Commun.* **2006**, *27*, 522.
(30) Ni, H.; Kawaguchi, H.; Endo, T. *Macromolecules* **2007**, *40*, 6370.
(31) Hoare, T.; Pelton, R. *Biomacromolecules* **2008**, *9*, 733.
(32) Taira, S.; Du, Y.-Z.; Kodaka, M. *Biotechnol. Bioeng.* **2006**, *93*, 396.
(33) Pan, X.; Yu, S.; Yao, P.; Shao, Z. *J. Colloid Interface Sci.* **2007**, *316*, 405.
(34) Hu, J.; Yu, S.; Yao, P. *Langmuir* **2007**, *23*, 6358.
(35) Das, M.; Mordoukhovski, L.; Kumacheva, E. *Adv. Mater.* **2008**, *20*, 2371.
(36) Nagai, S.; Ueda, A.; Toyoda, K. U.S. Patent 4,245,053, Jan 13, **1981**.
(37) Cavus, S.; Gürdag, G. *Ind. Eng. Chem. Res.* **2009**, *48*, 2652.
(38) Stuart, M. A. C. *Colloid Polym. Sci.* **2008**, *286*, 855.
(39) Wong, J. E.; Richtering, W. *Curr. Opin. Colloid Interface Sci.* **2008**, *13*, 403.
(40) Ohshima, H. *Colloid Polym. Sci.* **2007**, *285*, 1411.
(41) Radic, D.; Gargallo, L. *Macromolecules* **1997**, *30*, 817.
(42) Häntzschel, N.; Zhang, F.; Eckert, F.; Pich, A.; Winnik, M. *Langmuir* **2007**, *23*, 10793.
(43) Boyko, V.; Pich, A.; Lu, Y.; Richter, S.; Arndt, K.-F.; Adler, H.-J. *Polymer* **2003**, *44*, 7821.
(44) Demco, D. E.; Hafner, S.; Spiess, H. W. In *Handbook of Spectroscopy of Rubbery Materials*; Litvinov, V., De, P. P., Eds.; Repra Technology Ltd.: Shawbury, UK, 2002.
(45) Demco, D. E.; Blümich, B. *Encycl. Polym. Sci. Technol.* **2004**, *10*, 637.
(46) Spevacek, J. *Curr. Opin. Colloid Interface Sci.* **2009**, *14*, 184.
(47) Guillermo, A.; Cohen Addad, J. P.; Bazile, J. P.; Duracher, D.; Elaissari, A.; Pichot, C. C. *J. Polym. Sci., Part B: Polym. Phys.* **2000**, *38*, 889.
(48) Ru, G.; Wang, N.; Huang, S.; Feng, J. *Macromolecules* **2009**, *42*, 2074.
(49) Sotta, P.; Fülber, C.; Demco, D. E.; Blümich, B.; Spiess, H. W. *Macromolecules* **1996**, *29*, 6222.
(50) Patrickios, C. S. *J. Colloid Interface Sci.* **1995**, *175*, 256.
(51) Ho, B. S.; Tan, B. H.; Tan, J. P. K.; Tam, K. C. *Langmuir* **2008**, *24*, 7698.
(52) Bradley, M.; Vincent, B.; Burnett, G. *Aust. J. Chem.* **2007**, *60*, 646.
(53) Kleinen, J.; Richtering, W. *Macromolecules* **2008**, *41*, 1785.